

EPMA and LA-ICP-MS Data of Clinopyroxene and Chromite from the Wadi Ghadir Ophiolites, Eastern Desert, Egypt

B.A.Zoheir^{1,2}, A.A.Khalil², M.D.Feigenson³ and A.S.Diab¹

¹Geology Dept., Faculty of Science, Benha Univ., Benha, Egypt

²Institute of Geosciences, Kiel Univ., D-24118 Kiel, Germany

³Earth and Planetary Sciences Dept., Wright-Rieman Labs, Rutgers Univ., Piscataway, NJ, USA

E-Mail: Aliaadiab8@gmail.com

Abstract

New EPMA and LA-ICP-MS data of pyroxene and chromite are used to assess the so far published tectonic setting of Wadi Ghadir Ophiolite (WGO) in the Central Eastern Desert of Egypt. The low contents of TiO_2 (< 0.46 wt%) and high MgO (13.39-15.17 wt%) concentrations in the analyzed clinopyroxene suggest a depleted residual mantle source material. The trace element composition and REE patterns reflect transitional IAT-boninitic geochemical affinities in a supra-subduction zone setting. Chromite, on the other hand, shows high Cr#($Cr/(Cr+Al)$) (0.83-0.88 mol) and relatively constant Mg#($Mg/(Mg+Fe^{+2})$) (0.66-0.70 mol), indicating a high degree of partial melting of the uPP.er mantle source. These features are typical for supra-subduction zone in a back-arc or inter-arc basin setting. The micro-analytical data of relict magmatic mineral phases in the WGO and other ophiolitic rocks in the Arabian-Nubian Shield can help in interpreting their precise tectonic setting as far as data of the immobile, incompatible elements are used.

Keywords: EPMA, LA-ICP-MS, Pyroxene, Chromite, Ophiolites, Wadi Ghadir, Eastern Desert, Egypt.

1. Introduction

Ophiolites and ophiolitic melanges are the major components of Arabian Nubian Sheild (ANS) representing fragments of oceanic lithosphere obducted onto the continental crust during the amalgamation of the ANS [53]. They consist of a lower “mantle” unit of serpentized ultramafic rocks and an uPP.er “crustal” unit of layered and isotropic gabbro, sheeted dykes and pillow basalts. In the Egyptian Eastern Desert (ED), the Neoproterozoic ophiolites are typically composed of dismembered blocks in a tectonic mélange and widely distributed in the central and southern blocks of the ED. These rocks are commonly located along the major thrust faults [25] [26] [27], and particularly along the decollement and suture zones (e.g., Wadi Ghadir, Fawakhir area, El Rubshi, El-Degheimi area, Jebel Shilman area, Gebel Moqsim, Gebel EL Gerf, and Abu Dahr ophiolites) Fig (1). They have supra-subduction geochemical signatures (e.g., Fawakhir area [1]; Wadi Ghadir ophiolite [31] [1]; Abu Dahr ophiolite [34]; Wadi Semna [9] , but either forearc or backarc setting is remain controversial [1].

The Wadi Ghadir ophiolite in the Central Eastern Desert (CED) of Egypt was selected to envisage its mineralogical and geochemical characteristics as a well-constrained, heavily studied ophiolitic sequence in the ED.

2. Methods aPP.lied

The petrographic studies were carried out on a number of thin sections representations the various rock units exposed in the study areas. An Olympus BX51-P microscope was used to study and photograph the most fresh samples for their mineral components and textures.

2.1 Bulk rock trace element analyses by ICP-MS procedure

For each sample, ~100 mg of whole rock powder was digested in concentrated HF-HNO₃ followed by concentrated HNO₃ and then dried. Dried samples were re-dissolved and diluted in 2% ultrapure HNO₃, and subsequently analyzed by inductively coupled plasma mass spectrometry (ICP-MS) on a Thermo iCapQcTM mass spectrometer at Rutgers University. Three standards (BCR-2, BIR-1a, BHVO-2) were used to calibrate the instrument with regressions yielding r^2 values of at least 0.99 for all of elements measured. Each sample consisted of 10 main runs, with each run containing 10 sweeps of the desired mass range. An acid blank and calibration standards were analyzed every 15 samples to ensure instrument calibration. The instrument calibration was also monitored by analyzing the calibration standards as unknowns during the run.

Petrographic investigations were aided by SEM back-scattered electron imaging. Chemical composition of silicate and spinel (chromite) in the selected samples was determined on polished thin sections using a SX-50 Cameca instrument at the Technical University of Clausthal, Germany. Operating conditions for sulfides were a 20 keV accelerating voltage, with a 30 nA beam current (1 μm focused beam), and counting times of 10 to 100 sec. For silicate and chromite, the operating conditions were 15 kV, with a beam current of 10 to 20 nA, a beam size of 1 micron, and counting times of 20 seconds. Standards used were silicates, oxides, and pure elements.

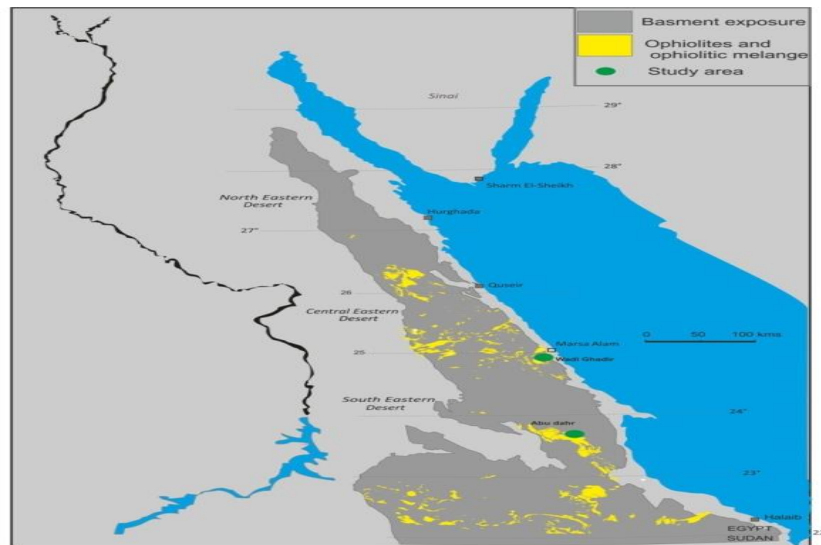


Fig (1) Distribution of the ophiolitic rocks in the Eastern Desert, Egypt
(Modified from Shackleton et al., 1980).

2.2 Trace elements in silicate by LA-ICP-MS

Laser ablation single collector ICP-MS analyses of pyroxene minerals were performed at the University of Kiel, using a 193 nm ArF excimer laser ablation system (GeoLasPro Plus, Coherent) coupled to an Agilent 7500s ICP-MS. Samples were loaded into a Zurich-type low dispersion high capacity laser ablation cell flushed with 1.0 L/min He as the carrier gas. Addition of 14 mL/min H₂ into the He carrier gas stream before entering the ablation cell led to an increase in sensitivity and reduction of oxide formation. The laser was run at a pulse frequency of 5 Hz and pulse energy of 2.6 J/cm² on the sample surface with a 50 µm spot size. The laser was automatically switched on for 60 seconds for signal acquisition and then off for 20 seconds for background levels to be attained and measured. To reduce the potential error from surface contamination, the first 5–10 s of each sample acquisition were discarded from data integration. The GLITTER software package was used for data reduction using the graphical visualization tool for setting integration intervals for each analyzed spot. In GLITTER external calibration was done with silicate glass NIST SRM612 using ⁴⁸Ca for internal standardization.

Ultramafic rocks are the most abundant and distinctive ophiolitic component, particularly at the base of the ophiolite which is widespread in a mélange forming large masses, reaching up to mountains as in Gebel Lawi, Gebel Lewiwi, Gebel Al-Anbaut and Gebel Ghadir, which are highly serpentinized Fig (2). Massive and schistose serpentinite crosscut by listvenite veins at Gebel Al-Anbaut, talc carbonate Fig (a), and magnesite pockets at Gebel Ghadir. Mainly relict of ultramafic rocks is still preserved along wadi

Saudi as peridotite and intruded by layered and meta-gabbro.

3. Geologic setting and study areas

In the CED, the best-exposed ophiolite sections in Wadi Ghadir, at Wadi El Beda and along Wadi Saudi, are considered a Penrose ophiolite sequence. It has been deformed and exposed by shear zones associated with the Najd transcurrent fault system and was emplaced by SE-NW directed thrusting. The Wadi Ghadir area is located in the Central Eastern Desert (CED) of Egypt, between latitudes 24°43'N and 24°49'N and longitudes 34°45'E and 35°00'. A detailed field study revealed that the study area is classified into ophiolitic and non-ophiolitic rocks comprising ultramafic/mafic rocks, metasediments, tectonically melange, island arc metavolcanic, meta volcaniclastics, leucogabbro, and late-to syn-tectonic granite rocks Fig(2). It has a series of WNW to NW trending brittle and ductile faults characterized the Najd system [52]. Wadi El Beda and Wadi Saudi are the best exposures of ophiolite in wadi Ghadir environ. They composed essentially of, from lower to upper, cumulate ultramafic rock peridotite, layered gabbro, deep-seated gabbro, a sheeted dyke complex and pillow lava basalt associated with a thin cap of deep-sea sedimentary rocks, it considered a Penrose ophiolite type Fig (3).

The best exposure of the metagabbros is at Wadi El Beda and along Wadi Saudi. The layered metagabbro is considered major unit Figs (4b-c), transitional upward into the massive coarse-grained metagabbro, micro metagabbro and the hypabyssal metagabbro at the top and transitional downward into trachygabbro and relatively unaltered metagabbro at the bottom.

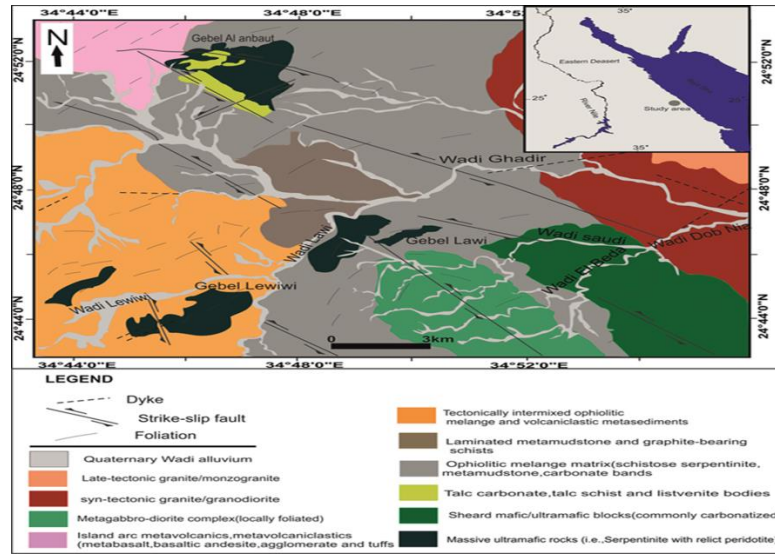


Fig (2) Geologic map of the Wadi Ghadir area (modified after Abd El Rahman et al., 2009).

The layered gabbro also exposed along the eastern part of Wadi Saudi. The layered gabbro considered as the major unit, which is clearly layered with white plagioclase and dark altered pyroxenes Fig (4c). They are intruded by calc-alkaline granitoid plutons at the eastern part of Wadi Ghadir area and closely associated with porphyritic pillow lavas at Wadi Saudi Fig (4b).

Sheeted dyke complexes, which are characterized by Penrose-type ophiolites of [21], are exclusively present in Wadi Ghadir ophiolite. They crop out along the southern part of Wadi El Beda Fig(4e) and the northeastern part of Gabal Ghadir. They show variation in composition from diabase to mafic, granophyre dykes also observed Fig (4d).

Pillow lavas are best preserved in Wadi Ghadir environ, which are exposed as vesicular pillow lavas in the southwestern part of Wadi El Beda closely associated with metabasalt Fig (4e), and as porphyritic pillow lavas at the Eastern part of Wadi Saudi closely associated with metagabbro Fig(4f). They have different shapes from rounded, oval, elliptical and circular with different size.

Metabasalt is associated with metagabbro and pillowed basalt at the western part of Wadi El Beda. While metasediment is exposed along Wadi Saudi associated with layered gabbro and relict of ultramafic rocks and is widespread in mélange around the western part of Wadi Ghadir as mudstone Fig (2).

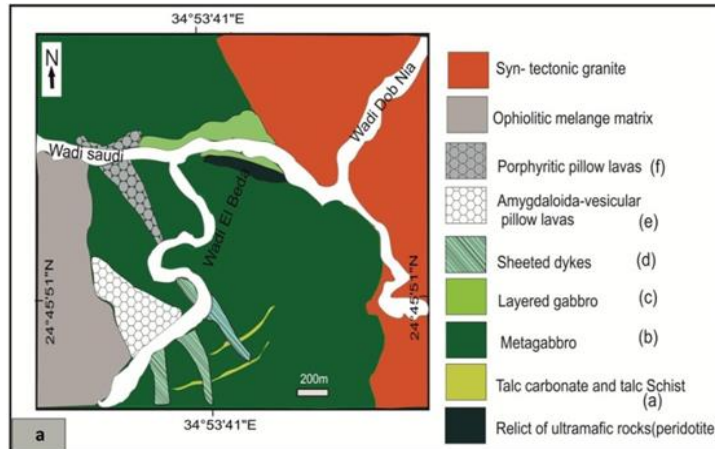


Fig (3) Geologic map of the best-exposed ophiolitic section at Wadi El Beda (modified after Abd El Rahman et al., 2009).



Fig (4) (a) Talc-carbonate in the ultramafic rock along shear zone at Wadi El Beda, (b) Metagabbros associated with metabasalt at wadi Saudi (looking E), (c) Layered metagabbros, (d) General view of sheeted dykes at the southern part of Wadi El Beda (looking N), (e) Vesicular pillow lavas in the southwestern part of Wadi El Beda (looking N), (f) Porphyritic pillow lavas at the Eastern part of Wadi Saudi closely associated with metagabbro.

4. Petrographic characteristics

Relict of ultramafic rocks is still preserved along Wadi Saudi as peridotite intruded by layered and metagabbro. They composed essentially of serpentine mineral (dominated by antigorite and lizardite), actinolite, and tremolite with relics of olivine and high abundance opaque minerals Fig(5a) including pyrite, chalcopyrite, and goethite. Serpentinites are composed essentially of lizardite, antigorite, sepiolite, brucite and Chromite with minor olivine and pyroxene relics and opaques Fig(5b). Sepiolite is a hydrous silicate mineral commonly associated with serpentine and occurs as yellow fibrous Fig(5b).

Metagabbro is the most abundant rocks in the Wadi Ghadir. The petrographic studies revealed that there are different varieties of the metagabbros basically composed of uralitic pyroxenes, partially altered plagioclase and opaque minerals with some accessory minerals. Mesocratic gabbro composed mainly of pyroxene (partly metamorphosed into actinolite and tremolite) and plagioclase (anorthite in composition and partly altered into albite and saussurite) with an abundance of opaque minerals Fig(5c). Isotropic metagabbros vary in grain size from coarse- to medium-grained having pyroxenes, plagioclase, amphibole, chlorite, and calcite, with apatite as a secondary mineral, and less amount of olivine with serpentine Fig (5d). Layered gabbro essentially consists of pyroxenes, kaolinite and epidote with altered plagioclase, opaques, apatite,

olivine relics, serpentine, garnet, talc, and anthophyllite Fig (5e). Trachygabbro essentially consists of plagioclase (altered into kaolinite, saussurite, and sericite), and pyroxenes (dominated by orthopyroxene and clinopyroxenes) with uralitic amphibole and olivine relics altered into talc with minor amounts of apatite.

Sheeted dykes are exclusively presented in Wadi Ghadir ophiolite and showing varying composition from diabase to mafic composition, as granophyre dykes also observed. The mafic dykes include a fine-grained metabasalt and rosette gabbro or gabbro-diorite sheeted dyke. Metabasalt composed mainly of plagioclase (occurs as laths partially altered to kaolinite, saussurite, and epidote) and pyroxenes (altered to actinolite) with amphibole and serpentine as secondary minerals Fig(5f). The rosette gabbro or gabbro-diorite sheeted dyke is composed mainly of plagioclase, pyroxenes, quartz, opaque and amphibole Fig (5g).

Pillow lavas are observed in Wadi Ghadir ophiolite as; vesicular pillow lavas, and porphyritic pillow lavas. Vesicular pillow lava is mainly composed of plagioclase occurs as laths, augite, chlorite, vesicles filled with calcite and other carbonates within glassy groundmass Fig (5h). Porphyritic pillow lava essentially composed of phenocrysts of plagioclase, pyroxenes, and amphibole set in cryptocrystalline groundmass formed of laths of kaolinized plagioclase Fig (5i).

5. Mineral chemistry

The magmatic differentiation processes from ultramafic(mantle) to mafic(crust) in deep within the spreading centres not only concentrate olivine and pyroxenes but also concentrate sulfides and chromite as magmatic ore deposits. These minerals formed in the oceanic crust that has been obducted over continental margins by different tectonic settings to form ophiolite. During alteration and metamorphism especially serpentinization, Cr-spinels and clinopyroxene are usually remains without significant changes giving fingerprint evidence of tectonic settings and magma types.

5.1 Pyroxenes

Pyroxene minerals occurring as preserved relicts in the WGO layered metagabbro were analyzed by EPMA for major elements and by LA-ICP-MS for trace and REE composition, in an attempt to investigate its tectonic setting. The data show the presences of clinopyroxene and orthopyroxene. The clinopyroxene composition ranges from $\text{En}_{48}\text{Fs}_{14}\text{Wo}_{30}$ to plagioclase has altered to zoisite (Zo) in the isotropic metagabbros, (e) a radiating anthophyllite (Ath), talc (Tlc), serpentine (Srp), and apatite (Ap) of layered gabbro, (f) Mineral compositions of metabasalt, (g) Rosette gabbro or gabbro-diorite composed essentially of zoned altered plagioclase and pyroxenes with quartz and opaque minerals, (h) Vesicular pillow lavas, (i) porphyritic pillow lavas.

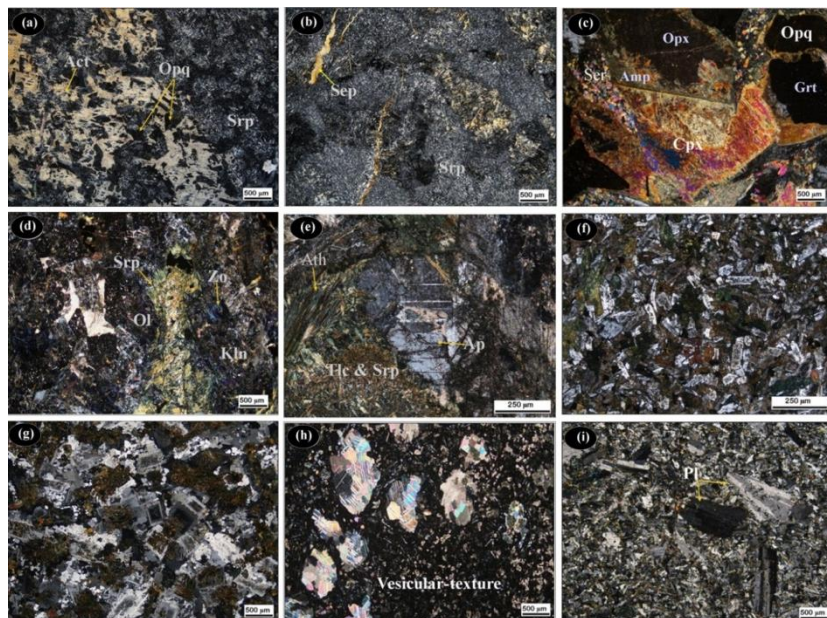
$\text{En}_{52}\text{Fs}_{17}\text{Wo}_{32}$, while the orthopyroxene from $\text{En}_{95}\text{Fs}_3\text{Wo}_0$ to $\text{En}_{96}\text{Fs}_4\text{Wo}_{0.15}$ Table (1-2). Augite and clinoenstatite are therefore the main pyroxene minerals

in the studied rocks Fig (6a). Temperatures of pyroxene crystallization calculated on basis of the two-pyroxene thermometer of range from 862-864°C and 1202-1220°C for orthopyroxene and clinopyroxene, respectively Fig (6b).

The clinopyroxenes are mainly high SiO_2 (51.15-53.66 wt. %), MgO (13.39-15.17 wt. %), and low TiO_2 (<0.46 wt. %) (Table 1), with the very low molecular Ti/Al (average 0.05) similar to back-arc basalts. Fig (7) shows that the clinopyroxene of the studied gabbroic rocks is low and very low-Ti-type based on the Ti content similar to samples from other supra-subduction zone-type ophiolites of Troodos, Vorinous, Pindos and Oman [11]. The relationship between the Al_2O_3 content of clinopyroxenes and the degree of silica saturation of the magma from which the crystals formed suggested that the studied clinopyroxenes' of layered gabbro gabbros have non-alkaline (sub-alkaline)

pyroxenes from the tholeiitic ocean-floor basalt, the tholeiitic within plate basalt and the volcanic arc basalt groups plot Based on the F 1 -F 2 discrimination diagram of [44], the plot in the within-plate tholeiitic basalt field Fig (8b) (Fig (8 c-d)

displays the compositional correspondence of clinopyroxenes from various ophiolitic basalts to those from oceanic actualistic equivalents (IAT and boninites-BON). It suggested that the clinopyroxenes of the gabbroic rocks of WGO are appropriate with those of island arc because of the low Ti and Na and high Si contents Fig (8c). Some samples are displaced towards the boninites because of the low Al content Fig (8d).



Fig(5) Photomicrographs of Wadi Ghadir ophiolite showing: (a) relict of ultramafics have serpentine (Srp), actinolite(Act) ,and a high abundant of opaque minerals, (b) fibrous sepiolite (Sep) associated with serpentine and actinolite (Act) in serpentinite, (c) Mesocratic gabbro consist of clinopyroxene (Cpx), orthopyroxene (Opx) partly altered to amphibole (Amp), (d) relics of olivine (Ol) still preserved with serpentine (Srp) at its rim,

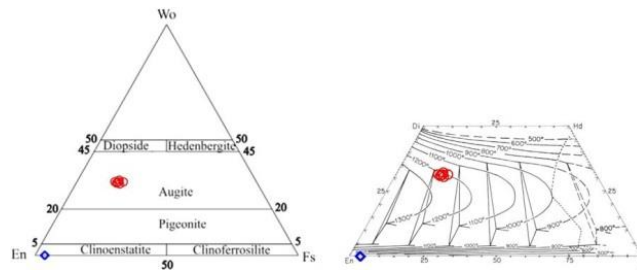


Fig (6) a) and b) Wo-En-Fs triangular diagram of compositions clinopyroxene of studied gabbroic rocks (after Morimoto et al., 1988).

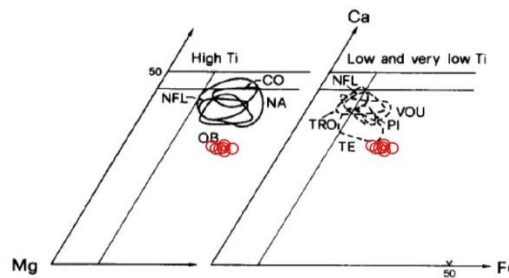


Fig (7) Ca-Mg-Fe (at.%) diagram for Ca-clinopyroxenes from high-Ti (left), low-Ti and very low-Ti (right) ophiolitic basalts. Abbreviations." NA = Northern Apennines; TRO = Troodos, PI= Pindos, VOU= Vourinos, NFL = Newfoundland, QB = Quebec; CO = Corsica (after Beccaluva et al., 1989).

Table (1) Representative EPMA data (wt. %) and calculated structural formulas of clinopyroxene from the Wadi Ghadir ophiolites.

| Sample/no | 3 / 1 . | 7 / 1 . | 10 / 1 . | 17 / 1 . | 18/1. | 23/1. | 27 / 1 . |
|------------------------------------------|-------------|-------------|-------------|-------------|-------------|-------------|-------------|
| SiO ₂ | 51.36 | 52.24 | 51.88 | 53.66 | 51.25 | 53.21 | 51.15 |
| TiO ₂ | 0.46 | 0.28 | 0.23 | 0.27 | 0.40 | 0.21 | 0.38 |
| Al ₂ O ₃ | 7.24 | 7.23 | 7.15 | 6.36 | 9.33 | 6.00 | 8.65 |
| FeO | 11.58 | 11.31 | 10.82 | 9.92 | 10.82 | 10.62 | 11.83 |
| MnO | 0.87 | 0.70 | 0.72 | 0.73 | 0.72 | 0.74 | 0.85 |
| MgO | 14.49 | 14.61 | 14.59 | 15.17 | 13.87 | 15.11 | 13.39 |
| CaO | 12.07 | 12.56 | 12.25 | 12.69 | 12.33 | 12.49 | 11.90 |
| Na ₂ O | 0.42 | 0.49 | 0.53 | 0.46 | 0.61 | 0.41 | 0.64 |
| K ₂ O | 0.10 | 0.07 | 0.07 | 0.14 | 0.16 | 0.11 | 0.07 |
| Cr ₂ O ₃ | 0.05 | 0.04 | 0.01 | 0.00 | 0.06 | 0.00 | 0.00 |
| Mole Proportions | | | | | | | |
| SiO ₂ | 0.85 | 0.87 | 0.86 | 0.89 | 0.85 | 0.89 | 0.85 |
| TiO ₂ | 0.01 | 0.00 | 0.00 | 0.00 | 0.01 | 0.00 | 0.00 |
| Al ₂ O ₃ | 0.07 | 0.07 | 0.07 | 0.06 | 0.09 | 0.06 | 0.08 |
| FeO | 0.16 | 0.16 | 0.15 | 0.14 | 0.15 | 0.15 | 0.16 |
| MnO | 0.01 | 0.01 | 0.01 | 0.01 | 0.01 | 0.01 | 0.01 |
| MgO | 0.36 | 0.36 | 0.36 | 0.38 | 0.34 | 0.37 | 0.33 |
| CaO | 0.22 | 0.22 | 0.22 | 0.23 | 0.22 | 0.22 | 0.21 |
| Na ₂ O | 0.01 | 0.01 | 0.01 | 0.01 | 0.01 | 0.01 | 0.01 |
| K ₂ O | 0.00 | 0.00 | 0.00 | 0.00 | 0.00 | 0.00 | 0.00 |
| Cr ₂ O ₃ | 0.00 | 0.00 | 0.00 | 0.00 | 0.00 | 0.00 | 0.00 |
| Sum | 1.69 | 1.71 | 1.69 | 1.72 | 1.69 | 1.71 | 1.67 |
| Cations on the basis of 6 oxygens | | | | | | | |
| Si | 1.91 | 1.92 | 1.92 | 1.96 | 1.88 | 1.96 | 1.89 |
| Ti | 0.01 | 0.01 | 0.01 | 0.01 | 0.01 | 0.01 | 0.01 |
| Al ^{IV} | 0.09 | 0.08 | 0.08 | 0.04 | 0.12 | 0.04 | 0.11 |
| Al ^{VI} | 0.22 | 0.23 | 0.24 | 0.23 | 0.28 | 0.22 | 0.27 |
| Al ^(total) | 0.32 | 0.31 | 0.31 | 0.27 | 0.40 | 0.26 | 0.38 |
| Fe ⁺⁺ | 0.36 | 0.35 | 0.34 | 0.30 | 0.33 | 0.33 | 0.37 |
| Mn | 0.03 | 0.02 | 0.02 | 0.02 | 0.02 | 0.02 | 0.03 |
| Mg | 0.80 | 0.80 | 0.81 | 0.82 | 0.76 | 0.83 | 0.74 |
| Ca | 0.48 | 0.49 | 0.49 | 0.50 | 0.48 | 0.49 | 0.47 |
| Na | 0.03 | 0.03 | 0.04 | 0.03 | 0.04 | 0.03 | 0.05 |
| K | 0.00 | 0.00 | 0.00 | 0.01 | 0.01 | 0.01 | 0.00 |
| Cr | 0.00 | 0.00 | 0.00 | 0.00 | 0.00 | 0.00 | 0.00 |
| Sum | 3.94 | 3.94 | 3.93 | 3.92 | 3.94 | 3.93 | 3.93 |
| Compositions | | | | | | | |
| Wo | 30.55 | 31.35 | 30.95 | 31.44 | 31.88 | 30.95 | 31.08 |
| En | 51.03 | 50.75 | 51.29 | 52.30 | 49.91 | 52.11 | 48.67 |
| Fs | 16.50 | 15.68 | 15.34 | 14.19 | 15.35 | 15.10 | 17.23 |
| Ac | 1.92 | 2.21 | 2.42 | 2.06 | 2.85 | 1.84 | 3.02 |
| Parameters | | | | | | | |
| Cr# | 0.00 | 0.00 | 0.00 | 0.00 | 0.00 | 0.00 | 0.00 |
| Mg# | 0.69 | 0.70 | 0.71 | 0.73 | 0.70 | 0.72 | 0.67 |
| T(G) | 1215.65 | 1212.21 | 1214.23 | 1217.56 | 1201.98 | 1220.50 | 1207.15 |

* Temperature is calculated based on pyroxene thermometer of Putirka (2008)

Table (2) Representative EPMA data (wt. %) and calculated structural formulas of orthopyroxene from the Wadi Ghadir ophiolites.

| Sample/no | 6/1. | 8/1. | 9/1. | 10/1. | 11/1. | 12/1. | 13/1. | 14/1. | 15/1. | 16/1. | 17/1. |
|------------------------------------------|-------|-------|-------|-------|-------|-------|-------|-------|-------|-------|-------|
| SiO ₂ | 41.39 | 41.15 | 41.52 | 41.51 | 41.21 | 40.93 | 40.89 | 41.11 | 41.29 | 41.30 | 40.86 |
| TiO ₂ | 0.01 | 0.02 | 0.00 | 0.01 | 0.00 | 0.00 | 0.03 | 0.01 | 0.01 | 0.00 | 0.01 |
| Al ₂ O ₃ | 0.00 | 0.00 | 0.01 | 0.01 | 0.00 | 0.01 | 0.00 | 0.01 | 0.00 | 0.00 | 0.00 |
| FeO | 8.52 | 8.64 | 8.07 | 8.29 | 8.73 | 8.90 | 8.93 | 7.87 | 8.31 | 7.75 | 8.05 |
| MnO | 0.10 | 0.14 | 0.16 | 0.14 | 0.13 | 0.11 | 0.12 | 0.15 | 0.16 | 0.16 | 0.13 |
| MgO | 50.70 | 50.60 | 50.85 | 50.68 | 50.40 | 50.32 | 49.83 | 50.94 | 50.98 | 51.08 | 50.96 |
| CaO | 0.00 | 0.00 | 0.00 | 0.00 | 0.03 | 0.00 | 0.00 | 0.04 | 0.00 | 0.00 | 0.11 |
| Na ₂ O | 0.00 | 0.01 | 0.02 | 0.02 | 0.00 | 0.02 | 0.00 | 0.01 | 0.01 | 0.01 | 0.00 |
| K ₂ O | 0.00 | 0.01 | 0.01 | 0.01 | 0.00 | 0.02 | 0.01 | 0.01 | 0.00 | 0.00 | 0.01 |
| Cr ₂ O ₃ | 0.01 | 0.01 | 0.01 | 0.00 | 0.00 | 0.02 | 0.01 | 0.00 | 0.00 | 0.00 | 0.00 |
| Mole Proportions | | | | | | | | | | | |
| SiO ₂ | 0.69 | 0.68 | 0.69 | 0.69 | 0.69 | 0.68 | 0.68 | 0.69 | 0.69 | 0.68 | |
| TiO ₂ | 0.00 | 0.00 | 0.00 | 0.00 | 0.00 | 0.00 | 0.00 | 0.00 | 0.00 | 0.00 | |
| Al ₂ O ₃ | 0.00 | 0.00 | 0.00 | 0.00 | 0.00 | 0.00 | 0.00 | 0.00 | 0.00 | 0.00 | |
| FeO | 0.12 | 0.12 | 0.11 | 0.12 | 0.12 | 0.12 | 0.12 | 0.11 | 0.12 | 0.11 | 0.11 |
| MnO | 0.00 | 0.00 | 0.00 | 0.00 | 0.00 | 0.00 | 0.00 | 0.00 | 0.00 | 0.00 | |
| MgO | 1.26 | 1.26 | 1.26 | 1.26 | 1.25 | 1.25 | 1.24 | 1.26 | 1.26 | 1.27 | 1.26 |
| CaO | 0.00 | 0.00 | 0.00 | 0.00 | 0.00 | 0.00 | 0.00 | 0.00 | 0.00 | 0.00 | |
| Na ₂ O | 0.00 | 0.00 | 0.00 | 0.00 | 0.00 | 0.00 | 0.00 | 0.00 | 0.00 | 0.00 | |
| K ₂ O | 0.00 | 0.00 | 0.00 | 0.00 | 0.00 | 0.00 | 0.00 | 0.00 | 0.00 | 0.00 | |
| Cr ₂ O ₃ | 0.00 | 0.00 | 0.00 | 0.00 | 0.00 | 0.00 | 0.00 | 0.00 | 0.00 | 0.00 | |
| Sum | 2.07 | 2.06 | 2.07 | 2.07 | 2.06 | 2.06 | 2.04 | 2.06 | 2.07 | 2.06 | 2.06 |
| Cations on the basis of 6 oxygens | | | | | | | | | | | |
| Si | 1.50 | 1.50 | 1.50 | 1.50 | 1.50 | 1.49 | 1.50 | 1.50 | 1.49 | 1.50 | 1.49 |
| Ti | 0.00 | 0.00 | 0.00 | 0.00 | 0.00 | 0.00 | 0.00 | 0.00 | 0.00 | 0.00 | 0.00 |
| Al ^{IV} | 0.50 | 0.50 | 0.50 | 0.50 | 0.50 | 0.51 | 0.50 | 0.50 | 0.51 | 0.50 | 0.51 |
| Al ^{VI} | 0.00 | 0.00 | 0.00 | 0.00 | 0.00 | 0.00 | 0.00 | 0.00 | 0.00 | 0.00 | 0.00 |

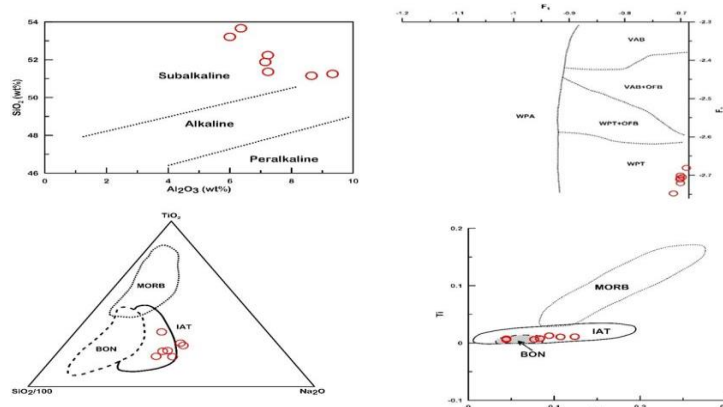


Fig (8) a) Al_2O_3 vs. SiO_2 of the studied clinopyroxene, field after Le Bas (1962), b) F_1 - F_2 discriminant functions for clinopyroxene analyses, discriminant boundaries after Nisbet and Pearse (1977), ocean-floor basalts (OFB), volcanic arc basalts (VAB), within plate tholeiitic basalts (WPT) and within plate alkalic basalts (WPA), c) and d) co-variation diagram of the analyzed clinopyroxenes in view of the tectonic settings (IAT: island arc tholeiite, BON: boninite, MORB: mid-ocean ridge basalt; after Beccaluva et al., 1989), c) $\text{TiO}_2\text{-Na}_2\text{O-SiO}_2/100$ (wt. %), d) Ti versus $\text{Al}^{(\text{IV})}$ (atomic ratios).

The LA-ICP-MS data of the clinopyroxene from show enrichment of their trace elements e.g., Rb (0.07 -1.6 PP.m), Ga (9-57 PP.m), Sr (5.7-99.9 PP.m), Y (8.9-60 PP.m), La (0.6-10 PP.m), Hf (0.2-3 PP.m), Th (0.06-0.7 PP.m), Nb (0.1 -7.8 PP.m) (Table 4) and have high abundance of LREEs (average 20.3 PP.m) rather than HREEs (average 18.4 PP.m). Thorium (Th) and Niobium Nb are the indicators for the crustal input because they are highly immobile from weathering to lower amphibolite facies metamorphism acting similarly during most petrogenetic processes [45].

While, in certain types of granulitic lower crust, Th may be depleted relative to Nb, and Nb tends to be mobile only in the deep melt at the highest temperatures or by very low degrees of melting [45]. Therefore, in the Nb/Yb versus Th/Yb tectonic discrimination diagram of Pearce (2008), the chemical composition of clinopyroxene of WGO gabbros plot distinctively away from the terrestrial MORB-OIB array consistent with the arc-backarc setting Fig (9a). Due to low Nb content, the clinopyroxene analytical data plot within the arc basalts field based on $\text{Hf}-\text{Th}-\text{Nb}$ tectono-magmatic discrimination diagram [59] Fig. (9b).

REE abundances in clinopyroxenes in the WGO gabbroic rocks are listed in Table 3. Chondrite-normalized REE patterns of these clinopyroxenes have flatter patterns with mild depletion in LREE Fig (9c), with $[(\text{Lu/La})_N < 10]$ that is comparable with clinopyroxene reported from Oman ophiolite (which is SSZ-type ophiolite) [51]. The concentrations of the most incompatible trace elements of these clinopyroxenes are also close to the primitive mantle abundances with positive K, Nb, Nd, Sm, and Ti Fig. (9b), referring to partial melting and mantle metasomatism [58].

5.2 Chromite

The chromite minerals of WGO were analyzed by electron microprobe for major oxides to better understand the petrogenesis and palaeotectonic environment of this type of ophiolite (Table 4). Their chemical composition revealed enrichment of Fe^{+2} (2.4-2.7) and low abundances of Fe^{+3} (0.4-0.7) indicating that chromite from gabbro relatively fresh with minor rim alteration. which, the Fe^{+2} and Fe^{+3} concentrations are relatively constant much across the rim and the core.

The Al–Cr– Fe^{3+} ternary diagram is to discriminate between diverse types of chromite (Fig. 10a; [12] shows that chromite data plot in the ophiolite field. The Cr– Fe^{3+} –Al ternary discrimination diagram of [54] shows the studied chromites are homogeneous in compositions that are similar to the Al-type chromites Fig (10b).

The high Cr/Cr+Al ratio that ranges from 0.83 to 0.88 and high and relatively constant Mg/Mg+ Fe^{2+} ratio that ranges from 0.66 to 0.70 of the chromite suggested a high degree of partial melting of the upper mantle source (Arai, [7]; Ishiwatari et al., [38]). In the Mg/Mg+ Fe^{2+} versus Cr/Cr+ Al diagram the composition of chromite from WGO is compared with the chromite composition from the Archean greenstone belts and the Archean layered complexes. Chromite

from these rocks has high Cr/Cr+Al ratio ranging from 0.83 to 0.87 and shows high and relatively constant Mg/Mg+ Fe^{2+} ratio to be between 0.63 and 0.64 wt%. The chromite compositions plot within Archean greenstone belts field close to Nuasahi Sukinda chromite Fig(10 c) and plot in ophiolitic chromite field Fig (10 d).

Both high Al and high Cr podiform chromitites are essentially presented in the central Eastern Desert ophiolite complexes, whereas the south Eastern Desert complexes only have high-Cr chromitites type [3].

Kamenetsky, et al., [39] stated that the TiO_2 and Al_2O_3 contents of chromite minerals are relatively controlled by magma composition. Therefore, they used their characteristic to define geodynamic settings in which the magma formed. The chromite data of WGO plot in the arc field overlapping with fields of SSZ peridotites Fig(11a). Also, the low titanium content revealed that the ophiolitic rocks formed in an arc-tectonic setting, and their chromite evolved in a supra-subduction zone arc setting.

In the Cr/Cr+Al versus TiO_2 tectonic discriminant diagram, chromite compositions plotted within IBM (IZU Bonin Mariana) field that indicates to transitional magma type between boninite and IAT and shows subduction related reaction Fig (11 b). An equation was proposed by Maurel & Maurel [42] used to calculate the Al_2O_3 contents of melts in equilibrium with chromite (equilibrium at 1 bar) as following: $[\text{Al}_2\text{O}_3]_{\text{spinel}} = 0.035 \times (\text{Al}_2\text{O}_3)_{\text{melt}}^{2.42}$. The Al_2O_3 contents of melts in the studied WGO chromites range from 8.1 to 9.7 wt%, are nearly similar the boninite melt in their compositions. Fig (11c) that shows the relation between Al_2O_3 content of the studied chromite and those of the melt suggesting their data plot very close to the evolutionary trend of an arc system Fig (11c; Kamenetsky, et al. [39]; Rollinson et al[50]). Franz and Wirth [33] used the Al_2O_3 - Cr_2O_3 relations to differentiate the arc cumulate spinels from mantle arrays, show that the WGO chromite is arc cumulate spinels Fig (11).

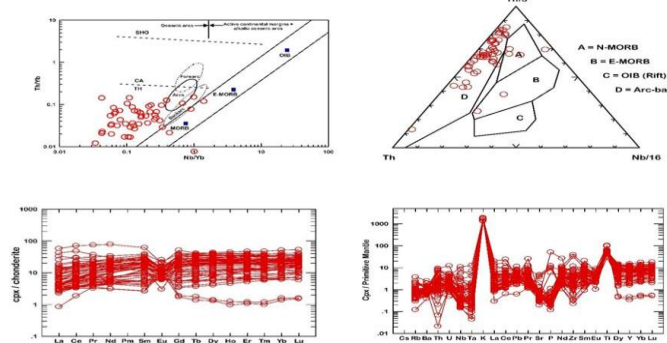


Fig (9) a) Th/Yb vs. Nb/Yb discrimination diagrams for clinopyroxene of WGO (Pearce, 2008), b) Hf–Th–Nb tectono-magmatic discrimination diagram (Wood, 1980), c) Chondrite-normalized REE patterns of the analyzed clinopyroxenes from WGO after Sun and McDonough (1989). d) Primitive mantle-normalized REE patterns of the analyzed clinopyroxenes from WGO after Sun and McDonough (1989).

Table (3) LA-ICP-MS analyses of clinopyroxene from the Wadi Ghadir ophiolites .

| sample | 128S304-1 | 128S304-2 | 129S304-3 | 130S304-4 | 131S304-5 | 132S304-6 | 133S304-7 | 134S301-1 | 135S301-2 | 136S301-3 | 137S301-4 | 138S301-5 | 139S301-6 | 140S301-7 | 141S301-8 | 142S303-2 | 143S303-3 | 144S303-4 | 145S303-5 | 146S303-6 | 147S303-7 | 148S303-8 | | 153S302-5 |
|------------|-----------|-----------|-----------|-----------|-----------|-----------|-----------|-----------|-----------|-----------|-----------|-----------|-----------|-----------|-----------|-----------|-----------|-----------|-----------|-----------|-----------|-----------|------|-----------|
| Ba | 6.12 | 8.26 | 7.65 | 7.53 | 4.89 | 13.41 | 9.99 | 17.53 | 6.66 | 4.15 | 4.29 | 7.89 | 6.40 | 4.64 | 8.72 | 6.15 | 7.94 | 3.72 | 6.07 | 4.48 | 4.23 | 5.06 | | 5.24 |
| Co | 119.62 | 185.77 | 90.27 | 89.90 | 107.84 | 116.93 | 95.78 | 277.73 | 117.03 | 87.80 | 92.00 | 106.43 | 143.45 | 112.96 | 118.64 | 98.23 | 133.76 | 105.44 | 124.83 | 121.83 | 112.88 | 156.65 | | 139.62 |
| Cu | 60.18 | 224.62 | 74.40 | 24.40 | 134.21 | 89.16 | 27.68 | 454.04 | 61.66 | 21.10 | 31.70 | 57.00 | 137.64 | 33.61 | 12.59 | 57.01 | 209.62 | 23.02 | 252.49 | 149.75 | 80.25 | 195.32 | | 171.49 |
| Ga | 13.81 | 26.06 | 11.70 | 10.23 | 13.92 | 14.11 | 9.19 | 41.89 | 15.54 | 11.01 | 11.02 | 13.34 | 20.29 | 13.81 | 17.70 | 11.71 | 15.53 | 13.93 | 14.58 | 12.83 | 12.68 | 19.14 | | 16.99 |
| Hf | 1.56 | 0.65 | 2.88 | 1.11 | 0.68 | 1.55 | 0.64 | 0.69 | 3.36 | 0.95 | 1.97 | 2.97 | 0.48 | 0.75 | 8.07 | 1.38 | 0.83 | 1.87 | 0.53 | 0.48 | 0.94 | 0.27 | | 0.39 |
| Li | 11.01 | 58.75 | 8.46 | 8.06 | 8.73 | 17.50 | 4.07 | 135.46 | 14.24 | 2.92 | 5.30 | 10.82 | 37.49 | 10.77 | 0.40 | 6.30 | 23.52 | 3.60 | 18.46 | 13.54 | 9.39 | 34.37 | | 30.69 |
| Nb | 0.66 | 0.61 | 2.17 | 0.26 | 0.13 | 0.33 | 0.25 | 27.71 | 0.61 | 0.88 | 0.76 | 1.06 | 0.22 | 0.18 | 7.87 | 1.60 | 0.18 | 2.15 | 0.17 | 0.15 | 0.11 | 0.18 | | 0.14 |
| Ni | 428.76 | 864.87 | 367.24 | 340.55 | 341.56 | 484.71 | 353.45 | 1355.37 | 478.25 | 334.74 | 435.49 | 434.28 | 624.69 | 350.54 | 561.48 | 351.13 | 589.80 | 422.36 | 509.82 | 502.00 | 434.99 | 676.64 | | 618.59 |
| P | 41.38 | 28.72 | 22.22 | 11.22 | 19.82 | 29.84 | 18.86 | 28.87 | 32.11 | 30.63 | 28.33 | 39.22 | 30.53 | 56.64 | 48.17 | 49.78 | 48.16 | 40.19 | 21.14 | 21.20 | 23.45 | 4819.15 | | 19.52 |
| Pb | 0.23 | 0.29 | 0.27 | 0.04 | 0.19 | 0.24 | 0.20 | 0.30 | 0.25 | 0.18 | 0.34 | 0.21 | 0.21 | 0.16 | 0.60 | 0.31 | 0.22 | 0.41 | 0.17 | 0.20 | 0.17 | 0.27 | | 0.18 |
| Rb | 0.35 | 1.18 | 0.74 | 1.56 | 0.44 | 0.92 | 0.40 | 2.39 | 0.67 | 0.22 | 0.48 | 0.67 | 0.75 | 0.26 | 1.34 | 0.54 | 0.41 | 0.23 | 0.64 | 0.35 | 0.38 | 0.50 | | 0.61 |
| Sc | 228.32 | 137.51 | 180.84 | 227.59 | 212.02 | 229.88 | 195.92 | 227.97 | 192.84 | 195.43 | 133.55 | 226.07 | 113.45 | 71.78 | 152.84 | 197.69 | 142.97 | 215.91 | 140.00 | 144.11 | 261.63 | 38.71 | | 106.30 |
| Sr | 11.34 | 14.60 | 17.52 | 7.06 | 10.23 | 41.33 | 8.62 | 27.97 | 10.68 | 7.70 | 8.09 | 11.48 | 14.74 | 10.80 | 5.78 | 10.27 | 19.43 | 7.05 | 11.78 | 9.64 | 8.76 | 13.49 | | 13.32 |
| Ta | 0.03 | 0.05 | 0.17 | 0.01 | 0.00 | 0.02 | 0.01 | 0.06 | 0.03 | 0.01 | 0.07 | 0.02 | 0.03 | 0.52 | 0.07 | 0.02 | 0.08 | 0.02 | 0.01 | 0.00 | 0.01 | | 0.01 | |
| Tb | 0.10 | 0.10 | 0.70 | 0.05 | 0.07 | 0.15 | 0.26 | 0.12 | 0.80 | 0.37 | 0.30 | 0.30 | 0.07 | 0.18 | 0.68 | 0.52 | 0.16 | 0.18 | 0.08 | 0.08 | 0.06 | 0.61 | | 0.10 |
| U | 0.03 | 0.05 | 0.12 | 0.01 | 0.02 | 0.04 | 0.03 | 0.05 | 0.06 | 0.08 | 0.04 | 0.03 | 0.09 | 0.06 | 0.04 | 0.04 | 0.03 | 0.09 | 0.03 | 0.09 | 0.02 | 0.09 | | 0.02 |
| V | 884.18 | 654.91 | 718.61 | 727.25 | 929.15 | 765.36 | 571.89 | 912.13 | 794.02 | 599.74 | 585.03 | 813.89 | 492.09 | 411.84 | 1073.94 | 724.94 | 584.40 | 721.91 | 470.68 | 410.35 | 864.14 | 406.15 | | 420.52 |
| Y | 52.47 | 16.00 | 46.57 | 26.91 | 29.16 | 41.59 | 20.99 | 15.56 | 50.39 | 28.91 | 37.79 | 50.14 | 8.34 | 19.46 | 68.90 | 37.36 | 53.26 | 9.27 | 8.96 | 23.54 | 57.85 | | 7.21 | |
| Zn | 194.39 | 315.89 | 150.39 | 135.65 | 176.08 | 193.15 | 158.63 | 472.24 | 188.02 | 150.46 | 187.27 | 170.07 | 238.58 | 189.05 | 275.25 | 167.54 | 215.87 | 213.88 | 207.69 | 202.62 | 185.60 | 280.18 | | 232.22 |
| Zr | 41.01 | 18.89 | 44.99 | 21.32 | 17.18 | 35.33 | 23.85 | 19.84 | 32.55 | 29.57 | 46.98 | 38.96 | 13.80 | 21.44 | 439.11 | 41.22 | 22.35 | 48.31 | 17.70 | 12.09 | 21.67 | 7.66 | | 11.23 |
| La | 1.97 | 1.04 | 2.17 | 0.20 | 0.72 | 0.10 | 0.84 | 0.76 | 0.86 | 2.39 | 3.34 | 2.82 | 1.07 | 2.17 | 6.09 | 2.09 | 0.62 | 3.23 | 0.65 | 0.67 | 0.62 | 13.63 | | 0.72 |
| Ce | 8.05 | 3.93 | 10.18 | 1.14 | 2.82 | 4.41 | 2.75 | 2.36 | 4.34 | 7.55 | 10.14 | 10.60 | 3.36 | 7.45 | 18.36 | 6.80 | 2.13 | 10.13 | 2.20 | 2.29 | 2.26 | 43.06 | | 2.28 |
| Pr | 1.68 | 0.64 | 1.82 | 0.34 | 0.61 | 0.93 | 0.53 | 0.38 | 0.98 | 1.23 | 1.76 | 2.03 | 0.50 | 1.23 | 2.95 | 1.26 | 0.35 | 1.63 | 0.39 | 0.40 | 0.47 | 7.04 | | 0.40 |
| Nd | 11.12 | 3.40 | 10.59 | 3.00 | 4.53 | 6.60 | 3.46 | 2.02 | 7.34 | 6.47 | 9.46 | 11.92 | 2.29 | 6.24 | 15.82 | 7.96 | 2.03 | 9.38 | 2.23 | 2.32 | 3.20 | 36.34 | | 2.07 |
| Sm | 5.01 | 1.23 | 4.14 | 2.39 | 3.43 | 1.57 | 0.69 | 3.92 | 2.30 | 3.25 | 4.48 | 0.63 | 1.79 | 5.89 | 3.36 | 0.92 | 4.17 | 0.79 | 0.85 | 1.77 | 9.38 | | 0.56 | |
| Eu | 0.85 | 0.54 | 0.72 | 0.18 | 0.44 | 0.57 | 0.37 | 0.36 | 0.59 | 0.58 | 0.57 | 0.88 | 0.49 | 0.53 | 1.27 | 0.90 | 0.34 | 0.91 | 0.36 | 0.38 | 0.35 | 1.16 | | 0.40 |
| Gd | 7.15 | 1.74 | 5.71 | 3.55 | 3.85 | 5.49 | 2.65 | 1.12 | 6.19 | 3.31 | 4.47 | 6.64 | 0.75 | 2.33 | 8.15 | 4.96 | 1.46 | 6.55 | 1.17 | 1.11 | 3.09 | 10.46 | | 0.70 |
| Tb | 1.34 | 0.34 | 1.08 | 0.71 | 0.74 | 1.07 | 0.52 | 0.23 | 1.23 | 0.65 | 0.85 | 1.21 | 0.15 | 1.53 | 0.93 | 0.29 | 1.27 | 0.22 | 0.21 | 0.59 | 1.54 | | 0.14 | |
| Dy | 9.24 | 2.53 | 7.66 | 5.08 | 5.36 | 7.48 | 3.80 | 2.09 | 8.79 | 4.76 | 6.11 | 8.70 | 1.15 | 3.07 | 11.00 | 6.54 | 2.16 | 9.01 | 1.50 | 1.47 | 4.22 | 9.57 | | 1.04 |
| Ho | 2.02 | 0.59 | 1.72 | 1.13 | 1.17 | 1.68 | 0.84 | 0.55 | 1.98 | 1.09 | 1.37 | 1.90 | 0.30 | 0.72 | 2.51 | 1.45 | 0.53 | 1.99 | 0.36 | 0.34 | 0.95 | 2.00 | | 0.26 |
| Er | 5.90 | 1.93 | 5.26 | 3.18 | 3.34 | 4.78 | 2.41 | 2.03 | 5.77 | 3.44 | 4.29 | 5.71 | 0.99 | 2.28 | 7.78 | 4.30 | 1.73 | 6.03 | 1.10 | 1.06 | 2.75 | 5.66 | | 0.85 |
| Tm | 0.85 | 0.30 | 0.81 | 0.45 | 0.47 | 0.68 | 0.35 | 0.33 | 0.82 | 0.52 | 0.67 | 0.82 | 0.17 | 0.34 | 1.21 | 0.61 | 0.28 | 0.88 | 0.17 | 0.16 | 0.39 | 0.70 | | 0.15 |
| Yb | 5.66 | 2.34 | 5.56 | 2.85 | 3.16 | 4.58 | 2.45 | 2.65 | 5.55 | 3.84 | 4.75 | 5.53 | 1.35 | 2.64 | 8.72 | 4.08 | 2.26 | 6.35 | 1.18 | 1.14 | 2.64 | 4.29 | | 1.13 |
| Lu | 0.81 | 0.35 | 0.81 | 0.37 | 0.44 | 0.68 | 0.39 | 0.44 | 0.82 | 0.61 | 0.76 | 0.83 | 0.23 | 0.41 | 1.35 | 0.58 | 0.38 | 0.96 | 0.19 | 0.18 | 0.41 | 0.62 | | 0.18 |
| Parameters | | | | | | | | | | | | | | | | | | | | | | | | |
| Σ REE | 61.64 | 20.90 | 58.23 | 24.12 | 30.04 | 43.39 | 22.94 | 16.00 | 49.18 | 38.75 | 51.78 | 64.06 | 13.43 | 31.61 | 92.62 | 45.82 | 15.48 | 62.50 | 12.51 | 12.58 | 23.71 | 145.45 | | 10.87 |
| Σ LREE | 28.68 | 10.78 | 29.62 | 8.61 | 11.51 | 16.96 | 9.52 | 6.56 | 18.03 | 20.53 | 28.52 | 32.73 | 8.33 | 19.40 | 50.38 | 22.37 | 6.39 | 29.45 | 6.63 | 6.91 | 8.67 | 110.61 | | 6.43 |
| Σ HREE | 32.96 | 10.12 | 28.61 | 17.31 | 18.53 | 26.44 | 13.41 | 9.44 | 31.15 | 18.22 | 23.27 | 31.34 | 5.09 | 12.21 | 42.25 | 23.46 | 9.09 | 33.04 | 5.88 | 5.67 | 15.04 | 34.84 | | 4.44 |
| Eu/Eu* | 0.44 | 1.14 | 0.46 | 0.21 | 0.45 | 0.40 | 0.56 | 1.27 | 0.37 | 0.65 | 0.46 | 0.49 | 2.19 | 0.79 | 0.56 | 0.68 | 0.91 | 0.54 | 1.16 | 1.21 | 0.46 | 0.36 | | 1.94 |
| (Lu/La)N | 3.97 | 3.29 | 3.64 | 17.87 | 6.03 | 6.45 | 4.50 | 5.62 | 9.31 | 2.47 | 2.21 | 2.84 | 2.11 | 1.83 | 2.15 | 2.71 | 6.03 | 2.89 | 2.79 | 2.62 | 6.40 | 0.44 | | 2.45 |

Table (3) continue

| sample | 154S302-6 | 155S302-7 | 156S307-1 | 157S307-2 | 158S307-3 | 159S307-4 | 160S307-5 | 161S308-1 | 162S308-2 | 163S308-3 | 164S308-4 | 165S308-5 | 167S308-7 | 168S308-8 | 169S308-9 | 170S308-10 | 171S309-1 | 172S309-2 | 173S309-3 | 17 |
|--------|-----------|-----------|-----------|-----------|-----------|-----------|-----------|-----------|-----------|-----------|-----------|-----------|-----------|-----------|-----------|------------|-----------|-----------|-----------|----|
|--------|-----------|-----------|-----------|-----------|-----------|-----------|-----------|-----------|-----------|-----------|-----------|-----------|-----------|-----------|-----------|------------|-----------|-----------|-----------|----|

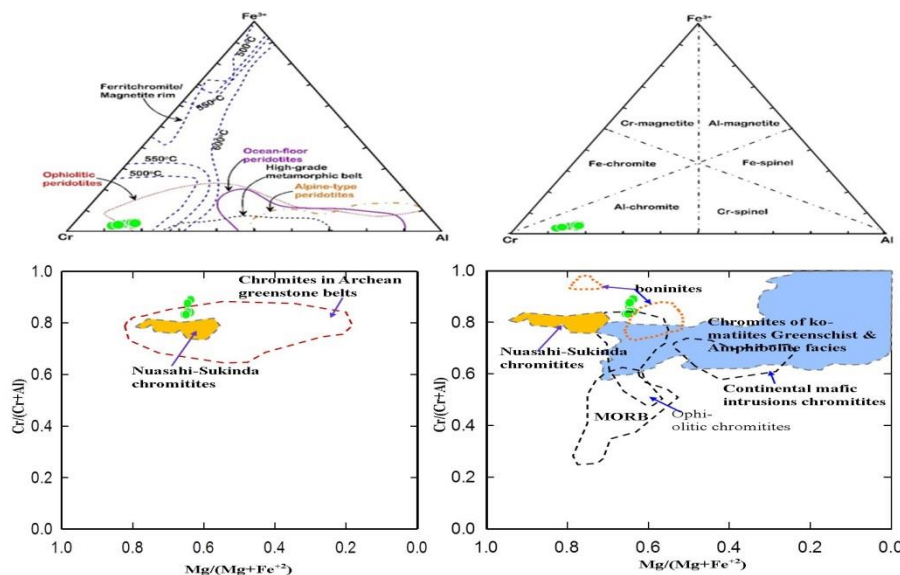


Fig (10) Tectonic discrimination diagrams for chromite of WGO. a) Cr-Fe³⁺-Al diagram (after Stevens, 1944) for the studied chromites, b) Cr/(Cr+Al) v. Mg/(Mg+Fe²⁺) (after Tamura and Arai, 2006), c) The Al-Cr-Fe³⁺ ternary diagram, which plot on the spinel stability boundary (Sack & Ghiorso, 1991), d) TiO₂ (wt%) v. Al₂O₃ (after Kamenetsky et al. 2001).

Table (4) Representative EPMA data (wt. %) and calculated structural formulas of chromite from the Wadi Ghadir ophiolites

| | 1 / 1. | 2 / 1. | 3 / 1. | 4 / 1. | 5 / 1. | 6 / 1. | 7 / 1. | 8 / 1. | 9 / 1. | 10 / 1. | 11 / 1. | 12 / 1. | 13 / 1. |
|-------------------------------------------------------------------------------------------------------|--------|--------|--------|--------|--------|--------|--------|--------|--------|---------|---------|---------|---------|
| Cr ₂ O ₃ | 62.31 | 61.92 | 65.93 | 63.58 | 61.97 | 62.68 | 62.78 | 62.06 | 62.16 | 62.33 | 62.19 | 65.09 | 62.45 |
| Al ₂ O ₃ | 8.24 | 8.45 | 5.60 | 7.14 | 8.33 | 8.22 | 8.44 | 8.37 | 8.22 | 8.02 | 7.97 | 6.28 | 8.54 |
| TiO ₂ | 0.06 | 0.09 | 0.10 | 0.07 | 0.09 | 0.10 | 0.11 | 0.08 | 0.11 | 0.08 | 0.07 | 0.08 | 0.10 |
| FeO | 14.57 | 13.77 | 14.01 | 13.98 | 14.48 | 14.46 | 13.91 | 14.46 | 14.00 | 14.72 | 14.15 | 13.85 | 14.13 |
| MgO | 14.46 | 14.58 | 13.69 | 14.22 | 14.51 | 14.27 | 14.38 | 14.68 | 14.54 | 14.45 | 14.42 | 14.07 | 14.62 |
| MnO corrected * | -0.25 | -0.25 | -0.26 | -0.25 | -0.25 | -0.25 | -0.25 | -0.25 | -0.25 | -0.25 | -0.25 | -0.26 | -0.25 |
| NiO | 0.09 | 0.02 | 0.00 | 0.04 | 0.10 | 0.02 | 0.08 | 0.06 | 0.05 | 0.07 | 0.05 | 0.08 | 0.07 |
| Total | 99.48 | 98.59 | 99.07 | 98.78 | 99.24 | 99.50 | 99.45 | 99.46 | 98.84 | 99.42 | 98.61 | 99.19 | 99.67 |
| Formula units based on 32 oxygens and Fe ²⁺ /Fe ³⁺ assuming full site occupancy | | | | | | | | | | | | | |
| Cr | 12.76 | 12.76 | 13.79 | 13.19 | 12.71 | 12.86 | 12.87 | 12.69 | 12.80 | 12.79 | 12.86 | 13.52 | 12.75 |
| Al | 2.52 | 2.60 | 1.75 | 2.21 | 2.55 | 2.51 | 2.58 | 2.55 | 2.53 | 2.45 | 2.46 | 1.95 | 2.60 |
| Ti | 0.01 | 0.02 | 0.02 | 0.01 | 0.02 | 0.02 | 0.02 | 0.02 | 0.02 | 0.02 | 0.01 | 0.02 | 0.02 |
| Fe ³⁺ | 0.69 | 0.60 | 0.42 | 0.56 | 0.70 | 0.58 | 0.51 | 0.72 | 0.62 | 0.72 | 0.65 | 0.50 | 0.61 |
| Fe ²⁺ | 2.48 | 2.41 | 2.68 | 2.51 | 2.45 | 2.56 | 2.51 | 2.42 | 2.43 | 2.48 | 2.45 | 2.55 | 2.45 |
| Mg | 5.58 | 5.67 | 5.40 | 5.56 | 5.61 | 5.52 | 5.56 | 5.66 | 5.64 | 5.59 | 5.62 | 5.51 | 5.63 |
| Mn | -0.05 | -0.05 | -0.06 | -0.06 | -0.05 | -0.06 | -0.06 | -0.05 | -0.05 | -0.05 | -0.06 | -0.06 | -0.05 |
| Ni | 0.02 | 0.00 | 0.00 | 0.01 | 0.02 | 0.01 | 0.02 | 0.01 | 0.01 | 0.02 | 0.01 | 0.02 | 0.02 |
| Total | 24.01 | 24.01 | 24.00 | 24.01 | 24.01 | 24.01 | 24.00 | 24.01 | 24.01 | 24.01 | 24.01 | 24.00 | 24.01 |
| Parameters | | | | | | | | | | | | | |
| Mg/Mg+Fe ²⁺ | 0.69 | 0.70 | 0.67 | 0.69 | 0.70 | 0.68 | 0.69 | 0.70 | 0.70 | 0.69 | 0.70 | 0.68 | 0.70 |
| Cr/Cr+Al | 0.84 | 0.83 | 0.89 | 0.86 | 0.83 | 0.84 | 0.83 | 0.83 | 0.84 | 0.84 | 0.84 | 0.87 | 0.83 |
| Fe ³⁺ /Cr+Al+Fe ³⁺ | 0.04 | 0.04 | 0.03 | 0.04 | 0.04 | 0.04 | 0.03 | 0.05 | 0.04 | 0.04 | 0.04 | 0.03 | 0.04 |
| Cr/Cr+Al+Fe ³⁺ | 0.80 | 0.80 | 0.86 | 0.83 | 0.80 | 0.81 | 0.81 | 0.80 | 0.80 | 0.80 | 0.81 | 0.85 | 0.80 |
| Mg# | 69.26 | 70.15 | 66.81 | 68.91 | 69.58 | 68.30 | 68.86 | 70.09 | 69.87 | 69.22 | 69.62 | 68.35 | 69.70 |
| Cr# | 83.53 | 83.08 | 88.76 | 85.66 | 83.30 | 83.64 | 83.30 | 83.26 | 83.53 | 83.90 | 83.95 | 87.42 | 83.07 |
| Al ₂ O ₃ in melt | 9.55 | 9.65 | 8.14 | 9.00 | 9.60 | 9.54 | 9.65 | 9.61 | 9.54 | 9.45 | 9.42 | 8.54 | 9.69 |

*Chromite recalculation inc. Fe²⁺/Fe³⁺ and Mn correction

6. Discussion and conclusions

The ophiolites have several varieties differ in their internal structure, geochemical makeup, and emplacement mechanism. Dilek and Furnes [21] reported that the ophiolites form in several tectonic

environments during the Wilson cycle evolution of ancient ocean basins from rift-drift and seafloor spreading stages to subduction initiation and closure phases. In the Egyptian Eastern desert, the Neoproterozoic ophiolites display subduction-related geochemical signatures (e.g., Fawakhir area; Wadi

Ghadir ophiolite; Abu Dahr ophiolite; Wadi Semna), but either forearc or back-arc setting remain

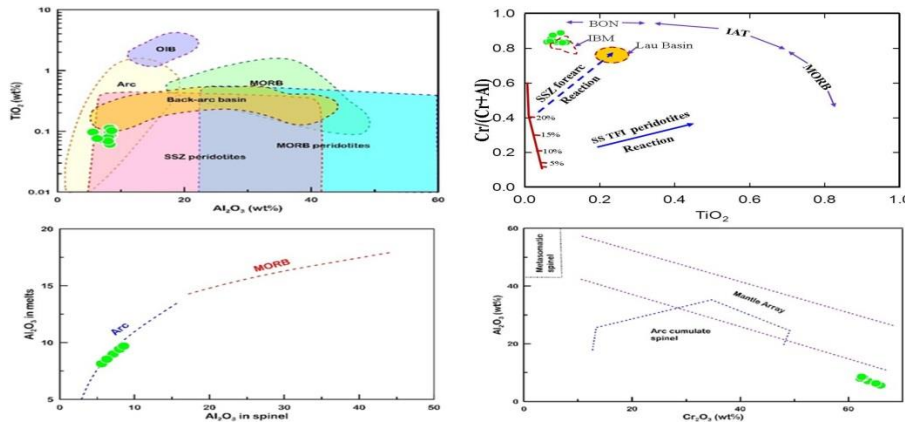
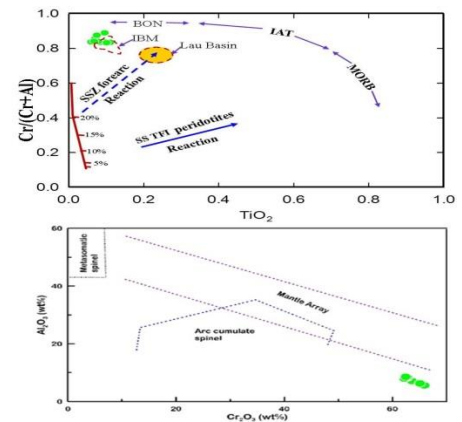


Fig (11)Tectonic discrimination diagrams for chromite of WGO. a) TiO_2 (wt%) v. Al_2O_3 (after Kamenetsky et al., 2001),, b) $\text{Cr}\#$ vs TiO_2 diagram of the composition of chromite after (Pearce et al., 2000), showing chromite composition plot within IBM field and have highly $\text{Cr}\# > 0.8$ wt%., c) Al_2O_3 in melts v. Al_2O_3 in spinel (after, Rollinson, 2010, based on melt calculations of Maurel & Maurel (1982), d) Al_2O_3 (wt%) v. Cr_2O_3 (wt%) (after Franz & Wirth, 2000).

Many authors (e.g. Farahat et al., [32]; Abd El-Rahman et al., [1]; Abd El-Rahman et al. [2]) studied WGO and stated that they were generated in a back-arc tectonic environment. In this work, an attempt to verify and assess the tectonic setting of Wadi Ghadir Ophiolite, using the microanalytical data of pyroxene and chromite is presented.

Generally, the Ti contents in the ophiolites reflect the parental magma type of the modern oceanic setting [11]. They classified into; high-Ti, low-Ti, and very low-Ti ophiolites. The high-Ti ophiolites match with MORB, while the low-Ti and very low-Ti ophiolites with the magmatic series of island-arc and boninitic types respectively, generated in the supra-subduction zone settings [11]. A water-bearing magma type is generated in the supra-subduction zone by a hydrous melting of the depleted uPP.er mantle source. Based on microprobe analysis of the clinopyroxenes of the layered gabbros of WGO, their non-alkaline affinity with the low Ti content indicate that they are commonly generated above a subduction zone in backarc basin setting, especially hot spots and continental graben structures . The low-Ti content of clinopyroxenes suggests crystallization of clinopyroxenes from a Ti-poor magma analogous to the low-Ti ophiolite group of .Also, these low-Ti and high-Mg content of the clinopyroxene may imply re-melting of depleted residual mantle source .Moreover, these clinopyroxenes are like those from the tholeiitic ocean-floor basalt, the tholeiitic within plate basalt and the volcanic arc basalt groups. This refers to these layered gabbros are supra-subduction zone ophiolites commonly having a Penrose type structural architecture. Their transitional IAT-boninitic geochemical affinities suggested that they were generated in back-arc basins

controversial (Stern et al. [53]; Azer and Stern [9]; Abd El-Rahman et al., [1]; Ali et al., [6]; Farahat [31].



show chemical characteristic having transitional within-plate basalt to island-arc basalt features formed in ensialic back-arc basins [32].

During alteration and metamorphism especially serpentinization, Cr-spinels are usually remains without significant changes and are not altered to secondary minerals, providing distinct information about magma compositions, melt- rock interaction, oxygen fugacity of the ophiolitic rocks, and used their compositions to explore their genesis and geodynamic setting (Arai and Yurimoto, [7]; Dick and Bullen, [19]; Rollinson, [50]).

In the subduction un-related setting, the fertile mantle character with Al-rich chromian spinels($\text{Cr}\# = \text{Cr}/(\text{Cr}+\text{Al}) < 0.6$ wt%/60 mol%) and relatively low oxygen fugacity (f_{O_2}), whereas in the subduction-related settings, the refractory mantle character with high Cr ratio >0.7 wt%/70 mol% of chromian spinel and high f_{O_2} are frequently found in magmatic rocks with a boninitic or a high -mg andesitic composition generated in arc environments(Zhou et al[61]; Arai et al., [7].

Chromite from the WGO ophiolites has high Cr ratio ($\text{Cr}/\text{Cr}+\text{Al}$) range from 0.83 to 0.87 and show high, relatively constant Mg ratio ($\text{Mg}/\text{Mg}+\text{Fe}^{+2}$) to be between 0.63 and 0.64, and shows a high Al-chromitites type, typical of chromite forming in a CED. Both high -Al and high-Cr podiform chromitites are common in the CED, whereas ophiolites in the SED are characterized by lower-Cr chromitites [3].

The chromite from Wadi Ghadir is similar to Nuasahi Sukinda chromite, India which has parental magma generated due to the interaction of a depleted mantle with a fluid-enriched melt possibly derived in response to the dehydration of a subducting slab).

The chemical compositions of chromite from WGO showing subduction-related setting plotted within SSZ field Fig (11 a). In the (Cr/Cr+Al) versus Mg(Mg+Fe⁺²) tectonic discriminant diagram, chromite compositions plotted within Nuasahi Sukinda field that indicates to backarc setting Fig(10 c and d). Neoproterozoic oceanic crust in Wadi Ghadir are generated in supra-subduction zone-backarc tectonic setting ,Wadi Ghadir ophiolite(WGO) has a back-arc geochemical signatures (Farahat et al., [32]; Abd El-Rahman et al., [1].

References

- [1] Y., Abd El-Rahman, A., Polat, Y., Dilek, B.J.,Fryer, M.,El-Sharkawy, and S.,Sakran, 2009a. Geochemistry and tectonic evolution of the Neoproterozoic Wadi Ghadir ophiolite, Eastern Desert, Egypt. *Lithos*, Vol.113,PP.. 158-178.
- [2] Y., Abd El-Rahman, A., Polat, Y.Dilek, , M.T., Kusky, M.,El-Sharkawi, and A.Said, 2012. Cryogenian ophiolite tectonics and metallogeny of the Central Eastern Desert of Egypt: International Geology Review, Vol.54,PP. 1870–1884.
- [3] A. H.;Ahmed, S.; Aria, and A. K.,Attia, 2001. Petrological characteristics of podiform chromitites and associated peridotites of Pan-African complexes of Egypt. *Miner. Dep*, Vol.36,PP..72–84.
- [4] A. F.Akinici, D.,Galadini, M.,Pantosti, L.,Petersen, Malagnini, and D. Perkins. 2009. Effect of time dependence on probabilistic seismic hazard maps and deaggregation for the central Apennines, Italy, *Bull. Seismol. Soc. Am.*, Vol.99,PP.. 585–610, doi:10.1785/0120080053.
- [5] M.,Akbulut, O.,Piskin, and, A.,Karayigit, 2006. The genesis of the carbonatized and silicified ultramafics known as listvenites: a case study from the Mihalıccık region (Eskisehir), NW Turkey. *Geological Journal*, Vol.41,PP.. 557-580.
- [6] K.A.,Ali, Azer, M.K., Gahlan, H.A., Wilde, S.A., Samuel, M.D. and Stern, R.J. 2010. Age of formation and emplacement of Neoproterozoic ophiolites and related rocks along the Allaqi Suture, south Eastern Desert, Egypt. *Gondwana Research*, Vol.18,PP. 583–595.
- [7] S., Arai, and Yurimoto, H., 1994. Podiform chromites of the Tari-Misaka ultramafic complex, southwestern Japan, as mantle-melt interaction products. *Econ Geol*, Vol.89,PP..1279–1288.
- [8] M., Auclair, Gauthier, M., Trottier, J., Jrbrak, M., Chartrand, F. 1993. Mineralogy, geochemistry, and paragenesis of the Eastern Metals serpentinite-associated Ni-Cu-Zn deposit, Quebec APP.alachians. *Econ. Geol*, Vol.88, PP.. 123-138.
- [9] M.K.,Azer, and Stern, R.J., 2007. Neoproterozoic (835-720 Ma) serpentinites in the Eastern Desert, Egypt: Fragments of fore-arc mantle. *The Journal of Geology*, Vol.115,PP.. 457–472.
- [10] M.K.,Azer, 2014. Petrological studies of Neoproterozoic serpentinitized ultramafics of the Nubian Shield: Spinel compositions as evidence of the tectonic evolution of Egyptian ophiolites: *Acta Geologica Polonica*, Vol.64,PP.. 113–127.
- [11] I.D., Baccaluva, Griolamo, P., Macciotta, G., and Morra, V. 1983. Magma affinities and fractionation trends in Ophiolites. *Ophioliti*, Vol.8, PP.. 307–324.
- [12] S.J., Barnes, P.L. Roeder, 2001. The Range of Spinel Compositions in Terrestrial Mafic and Ultramafic Rocks. *Journal of Petrology*, Vol.42,PP.. 2279–2302.
- [13] E., Bonatti, P.J. Michael, Mantle peridotites from continental rifts to ocean basins to subduction zones. *Earth and Planetary Science Letters*, Vol.91, pp.297–311, 1989.
- [14] Botros, N.S. 2002. Metallogeny of gold in relation to the evolution of the Nubian Shield in Egypt: *Ore Geology Reviews*, Vol.19, PP..137-164.
- [15] N.S., Botros, 2003. On the relationship between auriferous talc deposits hosted in volcanic rocks and massive sulfide deposits in Egypt: *Ore Geology Reviews*, Vol.23,PP..223–257.
- [16] N.S.,Botros, 2004. A new classification of the gold deposits of Egypt. *Ore Geology Reviews*, 25, 1–37.
- [17] Buisson, G., Leblanc, M. 1987. Gold in mantle peridotites from UPP.er Proterozoic ophiolites in Arabia, Mali, and Morocco. *Econ. Geol*, Vol.82,PP. 2091-2097.
- [18] D.P., Cox, D.A Singer., 1986. Grade and tonnage model of porphyry Cu-Au. In: Cox, D.P., Singer, D.A. (Eds.), *Mineral Deposit Models*. U.S. Geological Survey Bulletin, PP..110–114.
- [19] H.J.B., Dick, and T.Bullen, 1984. Chromian spinel as a petrogenetic indicator in abyssal and alpine-type peridotite and spatially associated lavas. *Contributions to* Evans, D., 2000. Stratigraphic, geochronological, and paleomagnetic constraints upon the Neoproterozoic climatic paradox. *Am. J. Sci.* 300, 347–433. *Mineralogy and Petrology*, Vol.86, PP..54-76.
- [20] Y., Dilek, and Furnes, H .2014. Ophiolites and their origins. *Elements*, 10: 93-100.
- [21] Y., Dilek, and Furnes, H., 2011. Ophiolites genesis and global tectonics: Geochemical and tectonic fingerprinting of ancient oceanic lithosphere. *Geological Society of American Bulletin*, Vol.123,PP.. 387-411.
- [22] R.M., El-Bayoumi, 1980. Ophiolites and associated rocks of Wadi Ghadir, east of Gabal Zabara, Eastern Desert, Egypt. PhD Thesis, Cairo University, Egypt, 171 PP..
- [23] A.,El-Dougoug, 1990. Gold anomalies in the Late Proterozoic felsic/mafic volcano-sedimentary sequence and associated rocks, Gebel Abu Marawat area, Eastern Desert, Egypt. *Bulletin of the Faculty of Science, Cairo University*, Vol.58,PP.. 533–548.
- [24] S., El-Gaby, S., List, F. K. and Tehrani, R., 1990. The basement complex of the Eastern Desert and Sinai. Ln: Said, R. (Ed.), *The Geology of Egypt*. Rotterdam, Balkema, PP..175-184.
- [25] S., El-Gaby, El-Nady, O., and A., Khudeir, 1984. Tectonic evolution of the basement complex in the

- Central Eastern Desert of Egypt: Geologische Rundschau, Vol.73, PP.. 1019–1036.
- [27] S., El-Gaby, List, F.K., and R., Tehrani, 1988. Geology, evolution and metallogenesis of the Pan-African belt in Egypt, in El-Gaby, S., and Greiling, R.O., eds., The pan-African belt of northeast Africa and adjacent areas: Tectonic evolution and economic aspects of a late Proterozoic orogeny: Braunschweig/Wiesbaden, Friedrich, Vieweg, Sohn Verlagsgesellschaft mbH, PP..17–68.
- [28] M.M.,El-Sayed, H., Furnes, F.H. Mohamed, 1999. Geochemical constraints on the tectono-magmatic evolution of the late Precambrian Fawakhir ophiolite, central Eastern Desert, Egypt. *j. Afr. Earth Sci.*, 29:515–533.
- [29] A.M., El-Mezayen, M.M., Hassan, M.,El-Hadad, M.M. Hassanein, 1995. Petrography, geochemistry and ore microscopy of Abu Marawat metavolcanics and associated gold mineralisation, North Eastern Desert, Egypt. *Bulletin of the Faculty of Science, Al-Azhar University*, 6 (2): 1999–2021.
- [30] M.P.,Escayola, J.A., Proenza, C., Van Staal, N., Rogers, T.,Skulski, 2009. The Point Rousse Listvenites, Baie Verte, Newfoundland: Altered ultramafic rocks with potential for gold mineralization? *Geological Survey, Report*, Vol.9, PP ..1-12.
- [31] E., S., Farahat, G., Hoinkes, and A.Mogessie, 2010. Petrogenetic and geotectonic significance of Neoproterozoic supra-subduction mantle as revealed by the Wizer ophiolite complex, Central Eastern Desert, Egypt. *International Journal of Earth Sciences*, Vol.100,PP..1433–1450.
- [32] Farahat, E.S., El Mahalawi, M.M. and Hoinkes, G. 2004. Continental back-arc basin origin of some ophiolites from the Eastern Desert of Egypt. *Mineralogy and Petrology*, Vol.82,PP..81–104.
- [33] L.,Franz, and R.,Wirth, 2000. Spinel inclusions in olivine of peridotite xenoliths from TUBAF seamount (Bismarck Archipelago/Papua New Guinea): evidence for the thermal and tectonic evolution of oceanic lithosphere. *Contributions to Mineralogy and Petrology* Vol.140, PP..283–95.
- [34] H.A., Gahlan, M.K., Azer, and A.E.S.,Khalil, 2015. The Neoproterozoic Abu Dahr ophiolite, South Eastern Desert, Egypt: petrological characteristics and tectono-magmatic Evolution. *Springer-Verlag Wien 2015*, Vol.109:PP..611-630.
- [35] W.L., Griffin, S.R., Shee, C.G., Ryan, T.T., Win, B.A,Wyatt,, 1999. Harzburgite to Iherzolite and back again: metasomatic processes in ultramafic xenoliths from the Wesselton kimberlite, Kimberley, South Africa. *Contributions to Mineralogy and Petrology* 134 (2 – 3), 232 – 250.
- [36] J.W.,Hawkins, 2003. Geology of supra-subduction zones—Implications for the origin of ophiolites, *in* Dilek, Y., and Newcomb, S., eds., *Ophiolite Concept and the Evolution of Geological Thought: Geological Society of America Special Paper*, 373: 227–268.
- [37] T. N. ,Irvine, 1965. Chromian spinel as a petrogenetic indicator. Part II, Petrographic applications, *Can J Earth Sci*, Vol.4,PP..71-103.
- [38] A;Ishiwatari, S.D., Sokolov, and S.V., Vysotskiy, 2003. Petrological diversity and origin of ophiolites in Japan and Far East Russia with emphasis on depleted harzburgite. In Dilek, Y, Robinson, P.T. (eds) *Ophiolites in earth history*. Geological Society of London Special Publication, 218: 597-617.
- [39] V.S., Kamenetsky, A.J., Crawford, and S., Meffre, 2001. Factors controlling chemistry of magmatic spinel: an empirical study of associated olivine, Cr-spinel and melt inclusions from primitive rocks. *J Petrol*, Vol.42,PP..655-671.
- [40] M., Leblanc, and W.,Fischer, 1990. Gold and platinum group elements in cobalt arsenide ores: Hydrothermal concentration from a serpentinite source-rock: *Mineralogy and Petrology*, Vol.42,PP.. 197–209.
- [41] M.J., Le Bas, 1962. The role of aluminium in igneous clinopyroxenes with relation to their parentage. *Am. J. Sci*, 260: 267– 288.
- [42] C.Maurel, andP, Maurel, 1982. Étude experimental de la distribution de l'aluminium entre bain silicate basique et spinel chromifère. Implications pétrogenétiques: tenore en chrome des spinelles. *Bulletin de Minéralogie*, Vol.105, PP..197–202
- [43] N, Morimoto,. 1988 Nomenclature of pyroxenes. *Mineral Petrol*, Vol.39,PP..55–7
- [44] E.G.Nisbet, 1974. The geology of the Neraida area, Othris mountains, Greece. Unpubl. PhD thesis, Univ. of Cambridge.
- [45] J.A., Pearce, 2008. Geochemical fingerprinting of oceanic basalts with aPPlications to ophiolite classification and the search for Archean oceanic crust. *Lithos* Vol.100,PP.. 14–48.
- [46] J.A, Pearce. 2014. Immobile element fingerprinting of ophiolites. *Elements* 10,101-108.
- [47] T.M.,Ramadan, 2002. Exploration for gold-bearing listwaenites at Um Khasila area, Central Eastern Desert, Egypt. *Egyptian Journal of Remote Sensing and Space Sciences*, Vol.5,PP. 63–76.
- [48] T.M., Ramadan, M.F., Sadek, I., Abu El Leil, and Salem, S.M. 2005. Um El Touyur El Fuqani gold mineralization, South Eastern Desert, Egypt: using Landsat ETM+ imagery. *Annals of Geological Survey of Egypt*, Vol.28,PP.. 263–281.
- [49] H.,Rollinson, 2005. Chromite in the mantle section of the Oman ophiolite: a new genetic model. *Island Arc*, Vol. 14,PP.. 542-550.
- [50] H.R., Rollinson, C.,Reid, and B.,Windley, 2010: Chromitites from the Fiskensæsset anorthositic complex, West Greenland: clues to late Archaean mantle processes; *in* The Evolving Continents: Understanding Processes of Continental Growth, T.M. Kusky, M.G. Zhai and W. Xiao, (ed.), Geological Society, London, Special Publications, Vol. 338,PP..197–212.

- [51] S.,Sano, J., Kimura, 2007. Clinopyroxene REE geochemistry of the Red Hills peridotite, New Zealand: interpretation of magmatic processes in the upper mantle and in the Moho Transition Zone. *Journal of Petrology* Vol.48 (1), PP..113–139. <http://dx.doi.org/10.1093/petrology/egl056>.
- [52] R.M., Shackleton, A.C., Ries, R.H., Graham, and W.R., Fitches, 1980. Late Precambrian ophiolite mélangé in the eastern desert of Egypt. *Nature*, Vol.285,PP.. 472–474.
- [53] R.J.,Stern, Johnson, P.R., Kroner, A. and Yibas, B. 2004. Neoproterozoic ophiolites of the Arabian-Nubian Shield. In: Kusky, T.M. (Ed.), *Precambrian Ophiolites and Related Rocks*. In: *Developments in Precambrian Geology*, Vol.13,PP.. 95–128.
- [54] R.E.,Stevens, 1944. Composition of some chromites of the western hemisphere. *American Mineralogist*, Vol.29,PP.. 1-34.
- [55] S.S., Sun, W.F. ,McDonough, 1989. Chemical and isotopic systematics of oceanic basalts: implications for mantle composition and processes. In: Saunders, A.D., Norry, M.J. (Eds.), *Magmatism in the Ocean Basins*. Geological Society, London, Special Publications, Vol.42,PP..313–345.
- [56] M.A., Takla, A.A. Suror, 1996. On the occurrence of Ni-sulphides and arsenides in some Egyptian serpentinites. *Egyptian Mineralogist*, Vol.8,PP.. 1–18.
- [57] A., Tamura, S.Arai, 2006. Harzburgite–dunite–orthopyroxenite suite as a record of supra-subduction zone setting for the Oman ophiolite mantle. *Lithos*, Vol.90, PP..43–56.
- [58] M.J. ,Walter, 1999. Melting residues of fertile peridotite and the origin of cratonic lithosphere. In: Fei, Y., Bertka, C., Mysen, B. (Eds.), *Mantle Petrology: Field Observations and High-Pressure Experimentation: A Tribute to Francis, R. (Joe) Boyd*. The Geochemical Society Special Publications, Houston, TX: PP..225 – 239
- [59] D.A. Wood, 1980. The application of a Th–Hf–Ta diagram to problems of tectonomagma Classification and establishing the nature of crustal contamination of basaltic lavas of the British Tertiary volcanic province. *Earth and Planetary Science Letters*, Vol.50,PP.. 11–30.
- [60] F., Zaccarini, G., Garuti, J.A., Proenza, Campos, L ., Thalhammer, O.A.R., Aiglsperger, T. & Lewis, J. F. 2011. Cr-spinel and platinum group elements mineralization in the Santa Elena ultramafic nappe (Costa Rica): geodynamic implications. *Geologica Acta*, Vol.9,PP.. 1–17.
- [61] M.F., Zhou, P.T., Robinson, and Malpas, J. and Liz. 1996. Podiform chromites in the Luobusa ophiolite (Southern Tibet): implications for melt–rock interaction and chromite segregation in the upper mantle. *J Petrol*, 37:3-21.
- [62] B.A.,Zoheir, and B.,Lehmann, 2011. Listvenite-lode association at the Barramiya gold mine, Eastern Desert, Egypt. *Ore Geology Reviews*, Vol.39,PP..101–115.

